Title: Control of polyunsaturated fatty acids desaturation by Sting regulates inflammatory responses

Authors: Isabelle K. Vila[1]*, Hanane Chamma[1], Alizée Steer[1], Clara Taffoni[1], Line S. Reinert[2], Evgenia Turtoi[3,4], Mathilde Saccas[1], Johanna Marines[1,5], Lei Jin[6], Xavier Bonnefont[7], Soren R. Paludan[2], Dimitrios Vlachakis[8,9,10], Andrei Turtoi[3,4], Nadine Laguette[1]*.

Affiliations:

[1] Institut de Génétique Humaine, CNRS, Université de Montpellier, Molecular Basis of Inflammation Laboratory, Montpellier, France

[2] Department of Biomedicine, University of Aarhus, Aarhus, Denmark

[3] Tumor Microenvironment Laboratory, Institut de Recherche en Cancérologie de Montpellier, Université de Montpellier, INSERM U1194, 34000 Montpellier, France

[4] Platform for Translational Oncometabolomics, Biocampus, CNRS, INSERM, Université de Montpellier, Montpellier, France.

[5] Azelead, 377 rue du Pr. Blayac, 34080 Montpellier

[6] Center for Immunology and Microbial Disease, Albany Medical College, Albany, NY 12208

[7] Institut de Génomique Fonctionnelle (IGF), University Montpellier, CNRS, INSERM, 34094 Montpellier, France

[8] Laboratory of Genetics, Department of Biotechnology, School of Applied Biology and Biotechnology, Agricultural University of Athens, 75 Iera Odos, 11855 Athens, Greece

[9] Division of Endocrinology and Metabolism, Center of Clinical, Experimental Surgery and Translational Research, Biomedical Research Foundation of the Academy of Athens, 11527 Athens, Greece

[10] University Research Institute of Maternal and Child Health & Precision Medicine, Medical School, National and Kapodistrian University of Athens, 11527 Athens, Greece

*Correspondence to: Nadine Laguette (Nadine.laguette@igh.cnrs.fr) and Isabelle K. Vila (Isabelle.vila@igh.cnrs.fr)

Abstract:
Inflammatory disorders are major health issues in which immune function and metabolic homeostasis are concertedly altered. Yet, how innate and metabolic pathways are coordinated, in homeostatic conditions, is poorly understood. Here, we demonstrate that the Stimulator of interferon genes (Sting) inhibits the Fatty acid desaturase 2 (Fads2) rate limiting enzyme in polyunsaturated Fatty acid desaturation, thereby controlling both Fatty acid (FA) metabolism and innate immunity. Indeed, we show that Sting activation increased Fads2 activity, while decreasing Fads2 levels enhanced Sting activation, establishing an anti-viral state. Remarkably, the cross-regulation between Sting and Fads2 is mediated by the cyclic GMP-AMP (cGAMP) Sting agonist and PUFAs. Indeed, PUFAs inhibit Sting activation, while cGAMP binds Fads2 and promotes its degradation. Thus, our study identifies Sting as a master regulator of the interplay between FA metabolism and inflammation.

One Sentence Summary: Sting inhibits polyunsaturated fatty acid metabolism.

Main Text:

The endoplasmic-reticulum (ER)-resident Stimulator of interferon genes (Sting) adaptor protein is central to the mounting of inflammatory responses in the presence of pathological nucleic acid species, including cytosolic dsDNA (*1*). Indeed, aberrant dsDNA accumulation under stress conditions (*2, 3*) or following pathogen infections (*4*) can be detected by the cyclic GMP-AMP (cGAMP) synthase (cGAS) (*5*), that catalyzes the production of cGAMP (*6, 7*). This second messenger interact with Sting (*8*), promoting its activation through the recruitment of the Tank binding kinase 1 (Tbk1), which mediates phosphorylation-dependent activation of transcription factors, such as the Interferon regulatory factor 3 (Irf3) (*9*). This signaling pathway triggers the production of inflammatory cytokines and type I Interferons (IFNs) (*1*). Dysregulations of Sting-associated signaling have been reported in a vast array of human pathologies. However, Sting function in absence of inflammatory challenge is unknown.

Because homeostasis requires tight regulation of metabolic and immune pathways (*10, 11*), we questioned the impact of Sting ablation on metabolic parameters, at steady-state. Under normal diet, wild-type (WT) and Sting$^{-/-}$ mice do not exhibit spontaneous inflammation (Fig. S1A), nor differences in body weight (Fig. 1A) and composition (Fig. S1B). Yet, Sting$^{-/-}$ mice present increased food intake (Fig. 1B) and improved insulin-independent glucose management as compared to WT mice (Fig. 1C and Fig. S1C-F), coupled to decreased hepatic gluconeogenesis (Fig. 1D and Fig. S1G). Indirect calorimetry measurements, using metabolic chambers, showed that Sting$^{-/-}$ mice have higher energy expenditure during the light phase (Fig. 1E and Fig. S1H), in absence of change in circadian rhythm (Fig. S1I) or spontaneous locomotor activity (Fig. S1J). Finally, Sting$^{-/-}$ mice, display increased thermogenesis (Fig. 1F), together with increased mRNA levels of the Uncoupling Protein 1 (Ucp1), that drives thermogenic activity in the adipose tissue (Fig. S1K) in agreement with recent published data (*12*). Importantly, metabolic phenotyping of cGas$^{-/-}$ and conditional myeloid cell-specific Sting$^{-/-}$ mice showed no significant alteration of measured metabolic parameters (Fig. S2). Therefore, our data demonstrate that absence of Sting leads to global metabolic improvement *in vivo*, independently of its canonical role in innate immunity. This further implies that non-immune cells likely drive metabolic changes observed in the absence of Sting.

To identify the molecular mechanism through which Sting regulates metabolic homeostasis, we performed tandem-affinity purification of Flag- and HA-tagged Sting (F/HA-Sting) stably expressed in mouse embryonic fibroblasts (MEF) knockout of Sting (MEF$^{Sting-/-}$). After migration on SDS-PAGE, immunopurified material was either silver-stained (Fig. 2A) or

Coomassie-stained for Mass spectrometry-based identification of Sting protein partners. Besides known Sting partners, such as Tbk1, this approach revealed a large number of proteins involved in metabolic pathways (Fig. S3A), notably including the RE-resident Fatty acid desaturase 2 (Fads2). Fads2 is the first, rate-limiting enzyme in the desaturation of linoleic acid [LA (18:2n-6, or Omega-6)] and α-linolenic acid [ALA (18:3n-3, Omega-3)] precursors (*13*), to generate polyunsaturated fatty acids (PUFAs) (Fig. S3B). Precisely, Fads2 catalyses the desaturation of ALA into eicosapentaenoic acid (EPA), and subsequently into docosahexaenoic acid (DHA). Desaturation of LA into dihomo-γ-linolenic acid (DGLA) also requires Fads2 (*13*), while further desaturation into arachidonic acid (AA) is catalysed by the Fatty acid desaturate 1 (Fads1) (*14*). Dedicated enzymes further process these PUFAs into Oxylipins that influence numerous physiological processes (*15*). The interaction between Fads2 and Sting was verified by Western blot (WB) analysis of Flag-immunoprecipitated F/HA-Sting (Fig. 2B). Conversely, Flag-immunoprecipitation of Flag-tagged Fads2 (F-Fads2) allowed co-immunoprecipitation of Sting, but not of Tbk1 (Fig. 2C). Thus, we show that Fads2 is a protein partner of Sting and that the interaction between Fads2 and Sting is independent of Tbk1. This further implies that recruitment of Fads2 to Sting does not require assembly of the Sting signalosome and therefore does not rely on pro-inflammatory stimulation.

We next questioned whether Sting influences Fads2 activity. Indeed, genetic association map analysis support a functional interaction between Fads2 and Sting (Fig. S3C). We used liquid chromatography coupled to mass spectrometry (LC-MS) to quantify PUFAs and their derivatives in liver samples from WT and Sting$^{-/-}$ mice. Partial least squares discriminant analysis (PLS-DA) of LC-MS data showed that WT and Sting$^{-/-}$ liver samples are significantly different (Fig. S4A). Correlation analysis showed a shift in PUFA content (Fig. S4B). Similar changes were observed upon quantification of PUFAs in WT and Sting$^{-/-}$ mice adipose tissue (Fig. S4C-D) or MEF (Fig. S4E-F). Although no significant shift in the total Omega-6/Omega-3 ratio was measured (Fig. 2D), calculating the total amount of derivatives from the main PUFAs families in liver samples, showed that absence of Sting leads to significantly increased levels of DGLA and DHA derivatives (Fig. 2E), that both result from Fads2 activity (*16*). Moreover, calculating the activity of Fads1 and Fads2 showed increased Fads2 activity in Sting$^{-/-}$ mice (Fig. 2F). Thus, absence of Sting leads to increased Fads2 activity *in vivo* and *in vitro*, establishing Sting as a negative regulator of Fads2. Importantly, the measured enrichments in Omega-3 PUFAs and derivatives are consistent with those from previous reports (*17-19*), and are sufficient to drive the metabolic improvements witnessed in Sting$^{-/-}$ mice (Fig. 1 and Fig. S1).

Because Sting activation leads to its degradation (*20, 21*), we next hypothesized that following activation, the Sting-dependent block to Fads2 activity would be alleviated. To test this hypothesis, we used dsDNA transfection to activate Sting-dependent signalling and consequent Sting degradation (Fig. 3A), prior to analysis of PUFAs. Similar to what was observed in the context of Sting ablation (Fig. 2), we observed an increase in PUFAs deriving from Fads2 activity, including DHA (Fig. 3B), without significant shift in the Omega-6/Omega-3 balance (Fig. 3C). Surprisingly, we observed that Fads2 protein levels are decreased following Sting activation (Fig. 3A). Similarly, infection with the Herpes Simplex Virus type I (HSV-1) DNA virus *in vitro* (Fig. S5A) and *in vivo* (Extended Data Fig. 5b-d), that induces Sting activation and degradation, also led to decreased Fads2 protein levels. Such decreased Fads2 levels have been previously reported as a consequence of its activation (*22*). Using cells knock-out of the IRF3 transcription factor downstream of STING, we verified that decreased FADS2 levels is not a consequence of type I

IFN production (Fig. S5E-F). Taken together, these data suggest that acute activation-dependent decrease of Sting levels promote Fads2 activity.

To assess the impact of chronic Sting activation on Fads2 activity, we used MEF knockout of the Three prime exonuclease 1 ($MEF^{Trex1-/-}$) that present with accumulation of endogenous cytosolic nucleic acid species and chronic Sting activation (*23*) (Fig. 3D). Surprisingly, Western blot analysis of whole cell extracts from WT-MEF and $MEF^{Trex1-/-}$ showed that absence of Trex1 correlates with a drastic decrease of Fads2 protein levels, despite no significant change in Sting protein levels (Fig. 3D). Analysis of PUFAs and derivatives in WT and $Trex1^{-/-}$ MEFs showed increased DGLA and DHA levels, supporting increased Fads2 activity (Fig. 3E). Increased levels of AA were also measured in this context (Fig. 3E), together with an increased Omega-6/Omega-3 ratio (Fig. 3F). Such accumulation of Omega-6 derivatives are expected to promote Sting-independent inflammatory processes (*24*). While this supports our model whereby Sting activation promotes increased Fads2 activity, this also indicates Sting degradation is not the sole parameter modulating Fads2 activity upon chronic Sting activation.

We thus investigated additional mechanisms that control Fads2 activity upon Sting activation. Because Sting activation requires its interaction with dinucleotides such as the cGAMP second messenger, and cGAMP levels are increased in $Trex1^{-/-}$ cells (Fig. S5G), we hypothesized that cGAMP may participate to control Fads2 activation. We assessed the validity of this hypothesis *in silico* by docking cGAMP and the 5,6-dimethylxanthenone-4-acetic acid (DMXAA) Sting agonist into Fads2. We used the resolved crystal of Sting in complex with cGAMP (PDB ID: 6WD4) and the molecular model of Fads2 as starting biological systems. This predicted that cGAMP and DMXAA can dock into Fads2, adopting similar conformation (Fig. 4a, left and central panels), achieving analogous interactions (Fig. S6) and docking energies (Table SI). We verified the interaction between cGAMP and Fads2 *in vitro*, using bead-immobilized biotinylated cGAMP and Flag-immunoprecipitated F-Fads2 or F/HA-Sting. Western blot analysis of bound proteins showed an enrichment of Fads2 to cGAMP (Fig. 4B). Next, we treated $cGas^{-/-}$, $Sting^{-/-}$, and WT-MEF with DMXAA, or performed dsDNA transfection to induce cGAMP production, prior to analysis of Fads2 levels by Western blot (Fig. 4C). This showed that Fads2 protein levels are decreased in presence of DMXAA, regardless of the expression of cGas and Sting, while dsDNA transfection led to significantly decreased Fads2 levels only in presence of cGas. These data confirm that Fads2 is a target of dinucleotides targeting Sting.

Intriguingly, molecular docking analysis between PUFAs (ALA, LA, DGLA, DHA, EPA and AA) and Sting, predict that PUFAs can dock to the cGAMP-binding domain of Sting (Fig. 4A, right panels). Indeed, we observed that cGAMP, DMXAA and PUFAs, adopt similar conformations in *in silico* docking experiments performed with Sting or Fads2 (Fig. S6 and S7A), achieving analogous binding energies (Table SI). Furthermore, Sting and Fads2 showed strong structural similarity, both with regards to the 3D arrangement of the docking site anatomy, and in terms of hydrophobicity, electrostatics and solvent accessibility (Fig. S6), suggesting that PUFAs are potential ligands of Sting. This prompted us to test the impact of administrating ALA (Omega-3) and LA (Omega-6) precursors to cells prior to assessment of DMXAA-induced Sting activation. Treatment with both ALA and LA led to decreased DMXAA-dependent stimulation of Interferon responses (Fig. 4D and Fig. S7B), establishing PUFAs are inhibitors of Sting. Consistently, knock-down of Fads2 led to increased *Ifn* expression (Fig. 4E and Fig. S7C), while antagonizing Fads2 using shRNAs or the sc26196 Fads2 inhibitor led to decreased infection by HSV-1 (Fig. 4F). This demonstrates that decreased Fads2 levels or activity contributes to endowing cells with an antiviral

status. Thus, we establish that PUFAs and cGAMP cooperate to regulate PUFA metabolism and Sting-dependent type I Interferon responses (Fig. S7E).

Altogether, we uncover a central role of Sting in the regulation of metabolic homeostasis, independently of its reported innate immune function. Indeed, we show that Sting is a negative regulator of Fads2 activity that thereby alters the desaturation of PUFAs. This process triggers cellular countermeasures to decreased Fads2 levels, likely to mitigate the potential deleterious impacts of imbalanced PUFAs pools and derivatives (*24*). We also demonstrate that Sting agonists can directly interact with Fads2 and promote its degradation, establishing Fads2 as a direct target of cGAMP. Thus, in chronic inflammatory pathologies, Sting-dependent modulation of Fads2 activity may feed metabolic comorbidities such as cachexia (*25*), while accumulation of AA and its derivatives can be expected to sustain Sting-independent pro-inflammatory processes (*26*). Furthermore, in therapeutic strategies targeting Sting (*27, 28*), alterations of Fads2 activity can be expected as a side effect. In parallel, that PUFAs can inhibit Sting, provides a previously unappreciated link between fatty acid metabolism and innate immune responses. Dietary habits, which impact the substrates provided to Fads2 for desaturation (*16, 29*), may therefore directly alter Sting activation and immune functions. Finally, we demonstrate that the crosstalk between Sting and Fads2 is regulates antiviral responses. Altogether, our findings offer unprecedented insight into the crosstalk between innate immune processes and metabolic regulation. Targeting this crosstalk in pathologies presenting with chronic inflammation, bears the promise to alleviate associated comorbidities.

References and Notes:

1. H. Ishikawa, Z. Ma, G. N. Barber, STING regulates intracellular DNA-mediated, type I interferon-dependent innate immunity. *Nature* **461**, 788-792 (2009).
2. J. Bai *et al.*, DsbA-L prevents obesity-induced inflammation and insulin resistance by suppressing the mtDNA release-activated cGAS-cGAMP-STING pathway. *Proceedings of the National Academy of Sciences of the United States of America* **114**, 12196-12201 (2017).
3. K. R. King *et al.*, IRF3 and type I interferons fuel a fatal response to myocardial infarction. *Nature medicine* **23**, 1481-1487 (2017).
4. D. Gao *et al.*, Cyclic GMP-AMP synthase is an innate immune sensor of HIV and other retroviruses. *Science (New York, N.Y.)* **341**, 903-906 (2013).
5. L. Sun, J. Wu, F. Du, X. Chen, Z. J. Chen, Cyclic GMP-AMP synthase is a cytosolic DNA sensor that activates the type I interferon pathway. *Science (New York, N.Y.)* **339**, 786-791 (2013).
6. P. Gao *et al.*, Cyclic [G(2',5')pA(3',5')p] is the metazoan second messenger produced by DNA-activated cyclic GMP-AMP synthase. *Cell* **153**, 1094-1107 (2013).
7. A. Ablasser *et al.*, cGAS produces a 2'-5'-linked cyclic dinucleotide second messenger that activates STING. *Nature* **498**, 380-384 (2013).
8. X. Zhang *et al.*, Cyclic GMP-AMP containing mixed phosphodiester linkages is an endogenous high-affinity ligand for STING. *Molecular cell* **51**, 226-235 (2013).
9. S. Liu *et al.*, Phosphorylation of innate immune adaptor proteins MAVS, STING, and TRIF induces IRF3 activation. *Science (New York, N.Y.)* **347**, aaa2630 (2015).
10. M. D. Buck, R. T. Sowell, S. M. Kaech, E. L. Pearce, Metabolic Instruction of Immunity. *Cell* **169**, 570-586 (2017).

11. J. R. Brestoff, D. Artis, Immune regulation of metabolic homeostasis in health and disease. *Cell* **161**, 146-160 (2015).
12. J. Bai *et al.*, Mitochondrial stress-activated cGAS-STING pathway inhibits thermogenic program and contributes to overnutrition-induced obesity in mice. *Communications biology* **3**, 257 (2020).
13. M. T. Nakamura, T. Y. Nara, Structure, function, and dietary regulation of delta6, delta5, and delta9 desaturases. *Annual review of nutrition* **24**, 345-376 (2004).
14. A. E. Leonard *et al.*, cDNA cloning and characterization of human Delta5-desaturase involved in the biosynthesis of arachidonic acid. *The Biochemical journal* **347 Pt 3**, 719-724 (2000).
15. M. Gabbs, S. Leng, J. G. Devassy, M. Monirujjaman, H. M. Aukema, Advances in Our Understanding of Oxylipins Derived from Dietary PUFAs. *Advances in nutrition (Bethesda, Md.)* **6**, 513-540 (2015).
16. F. Tosi, F. Sartori, P. Guarini, O. Olivieri, N. Martinelli, Delta-5 and delta-6 desaturases: crucial enzymes in polyunsaturated fatty acid-related pathways with pleiotropic influences in health and disease. *Advances in experimental medicine and biology* **824**, 61-81 (2014).
17. F. Capel *et al.*, DHA at nutritional doses restores insulin sensitivity in skeletal muscle by preventing lipotoxicity and inflammation. *The Journal of nutritional biochemistry* **26**, 949-959 (2015).
18. H. Yanai *et al.*, An Improvement of Cardiovascular Risk Factors by Omega-3 Polyunsaturated Fatty Acids. *Journal of clinical medicine research* **10**, 281-289 (2018).
19. M. Fernández-Galilea, E. Félix-Soriano, I. Colón-Mesa, X. Escoté, M. J. Moreno-Aliaga, Omega-3 fatty acids as regulators of brown/beige adipose tissue: from mechanisms to therapeutic potential. *Journal of physiology and biochemistry* **76**, 251-267 (2020).
20. H. Konno, K. Konno, G. N. Barber, Cyclic dinucleotides trigger ULK1 (ATG1) phosphorylation of STING to prevent sustained innate immune signaling. *Cell* **155**, 688-698 (2013).
21. Y. Wang *et al.*, TRIM30α Is a Negative-Feedback Regulator of the Intracellular DNA and DNA Virus-Triggered Response by Targeting STING. *PLoS pathogens* **11**, e1005012 (2015).
22. J. C. Ralston, S. Matravadia, N. Gaudio, G. P. Holloway, D. M. Mutch, Polyunsaturated fatty acid regulation of adipocyte FADS1 and FADS2 expression and function. *Obesity (Silver Spring, Md.)* **23**, 725-728 (2015).
23. A. Ablasser *et al.*, TREX1 deficiency triggers cell-autonomous immunity in a cGAS-dependent manner. *Journal of immunology (Baltimore, Md. : 1950)* **192**, 5993-5997 (2014).
24. J. K. Innes, P. C. Calder, Omega-6 fatty acids and inflammation. *Prostaglandins, leukotrienes, and essential fatty acids* **132**, 41-48 (2018).
25. H. Baazim *et al.*, CD8(+) T cells induce cachexia during chronic viral infection. *Nature immunology* **20**, 701-710 (2019).
26. M. Arita, Mediator lipidomics in acute inflammation and resolution. *Journal of biochemistry* **152**, 313-319 (2012).
27. S. M. Haag *et al.*, Targeting STING with covalent small-molecule inhibitors. *Nature* **559**, 269-273 (2018).

28. J. J. Wu, L. Zhao, H. G. Hu, W. H. Li, Y. M. Li, Agonists and inhibitors of the STING pathway: Potential agents for immunotherapy. *Medicinal research reviews* **40**, 1117-1141 (2020).
29. L. Galland, Diet and inflammation. *Nutrition in clinical practice : official publication of the American Society for Parenteral and Enteral Nutrition* **25**, 634-640 (2010).
30. L. Jin et al., STING/MPYS mediates host defense against Listeria monocytogenes infection by regulating Ly6C(hi) monocyte migration. Journal of immunology (Baltimore, Md. : 1950) 190, 2835-2843 (2013).
31. I. K. Vila et al., A muscle-specific UBE2O/AMPKalpha2 axis promotes insulin resistance and metabolic syndrome in obesity. JCI Insight 4, (2019).
32. I. K. Vila et al., Immune cell Toll-like receptor 4 mediates the development of obesity- and endotoxemia-associated adipose tissue fibrosis. Cell Rep 7, 1116-1129 (2014).
33. K. Abitbol et al., Clock-dependent and system-driven oscillators interact in the suprachiasmatic nuclei to pace mammalian circadian rhythms. PLoS One 12, e0187001 (2017).
34. L. S. Reinert et al., Brain immune cells undergo cGAS-STING-dependent apoptosis during herpes simplex virus type 1 infection. J Clin Invest, (2020).
35. J. Chong, D. S. Wishart, J. Xia, Using MetaboAnalyst 4.0 for Comprehensive and Integrative Metabolomics Data Analysis. Curr Protoc Bioinformatics 68, e86 (2019).
36. D. Warde-Farley et al., The GeneMANIA prediction server: biological network integration for gene prioritization and predicting gene function. Nucleic Acids Res 38, W214-220 (2010).
37. S. Vilar, G. Cozza, S. Moro, Medicinal chemistry and the molecular operating environment (MOE): application of QSAR and molecular docking to drug discovery. Curr Top Med Chem 8, 1555-1572 (2008).
38. D. Vlachakis, D. Tsagrasoulis, V. Megalooikonomou, S. Kossida, Introducing Drugster: a comprehensive and fully integrated drug design, lead and structure optimization toolkit. Bioinformatics 29, 126-128 (2013).

Acknowledgments: We thank Monsef Benkirane, Giacomo Cavalli, Jérôme Déjardin and Bernard de Massy for discussions and comments. **Funding:** Work in N.L.'s laboratory is supported by grants from the European Research Council (ERC-Stg CrIC: 637763, ERC-PoC DIM-CrIC: 893772), "LA LIGUE pour la recherche contre le cancer" and the "Agence Nationale de Recherche sur le SIDA et les Hépatites virales" (ANRS). H.C. is supported by a PhD fellowhip from" LA LIGUE pour la recherche contre le cancer". C.T. was supported by Merck Sharp and Dohme Avenir (MSD-Avenir – GnoSTic) program, followed by an ANRS fellowship. J.M. is supported by a "Conventions Industrielles de Formation par la Recherche" (CIFRE) fellowship from the "Agence Nationale de Recherche Technologie" (ANRT). A.S. is supported by the ERC-PoC DIM-CrIC (893772). I.K.V. was supported by the European Research Council (637763) followed by the "Prix Roger PROPICE pour la recherche sur le cancer du pancreas" of the Fondation pour la Recherche Médicale (FRM). We acknowledge the SIRIC Montpellier Cancer Grant INCa_Inserm_DGOS_12553 for support. We acknowledge Metamus-RAM and iExplore-RAM animal facilities. We thank the "Laboratoire de Mesures Physiques" of the University of Montpellier, for access to the Mass Spectrometry instruments. We thank Ross Tomaino from the "Taplin Mass Spectrometry Facility" of the Harvard Medical School, for Mass Spectrometry

analysis. Work in S.R.P.'s laboratory is supported by the European Research Council (ERC-AdG ENVISION; 786602), The Novo Nordisk Foundation (NNF18OC0030274), and the Lundbeck Foundation (R198-2015-171; R268-2016-3927). Work in A.T.'s laboratory is supported by a SIRIC Montpellier Cancer Grant INCa_Inserm_DGOS_12553, the Foundation de France (grant no. 00078461) and a LabEx MabImprove Starting Grant. X.B. is supported by ANR GH-gen (ANR-18-CE14-0017)**.**

Author contributions: I.K.V. and N.L conceived the study and designed experiments; I.K.V, H.C., A.S., C.T., L.S.R.., E.T., M.S., J.M., X.B., D.V., A.T. performed experiments; I.K.V. performed *in vivo* experiment, flag immunoprecipitation and immunoblotting, pull-down experiments, *in vitro* virus experiments, fads2 inhibitor experiments, 293T experiments; H.C. performed shRNA experiments; A.S. performed Trex1$^{-/-}$ MEF experiments; C.T. performed T98G experiments; E.T. performed PUFAs/oxylipins measurements; M.S. performed MEF dsDNA transfection and DMXAA experiments; J.M. performed virus production; X.B. performed locomotor activity and circadian rhythm *in vivo* experiments; L.S.R. performed *in vivo* virus infection; D.V. performed modelling and docking experiments, A.T. performed PUFAs/oxylipins measurements and statistical analysis. I.K.V., S.R.P., D.V., A.T. and N.L. supervised the study. J.L. provided mice and mice tissues samples. I.K.V., D.V., A.T. and N.L. analyzed data and prepared figures; I.K.V, D.V, A.T. and N.L. wrote the manuscript. All authors read and approved the final version of the manuscript.

Competing interests: The authors declare no competing interest.

Data and materials availability: All raw data and materials generated in the course of the present work are available upon request. Requests should be addressed to N.L. (Nadine.laguette@igh.cnrs.fr) or I.K.V. (Isabelle.vila@igh.cnrs.fr)

Supplementary Materials:

Materials and Methods

Figures S1-S7

Tables S1

References (*30-38*)

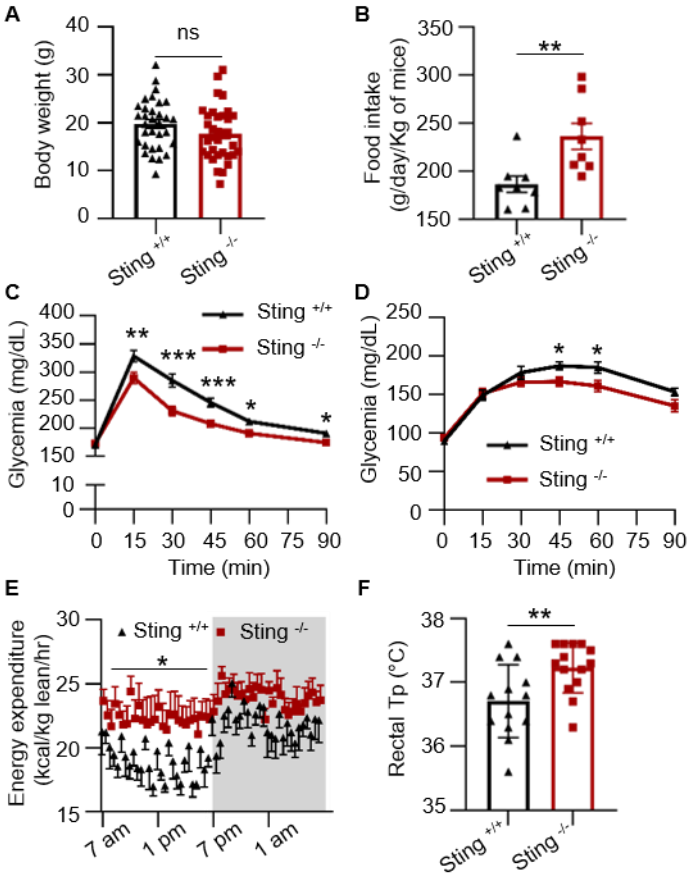

Fig. 1. Sting deficiency leads to global metabolic improvement.

(A) The body weight of Sting$^{+/+}$ (n=32) and Sting$^{-/-}$ (n=34) mice fed normal chow diet was measured at 8 weeks age. (B) Food intake of Sting$^{+/+}$ (n=8) and Sting$^{-/-}$ (n=9) mice. (C) Glucose tolerance test (GTT) was performed in Sting$^{+/+}$ (n=25) and Sting$^{-/-}$ (n=24) mice. (D) Pyruvate tolerance test (PTT) was performed in Sting$^{+/+}$ (n=7) and Sting$^{-/-}$ (n=7) mice. (E) The energy expenditure during day (white) and night (grey) per kg of lean mass of Sting$^{+/+}$ (n=6) and Sting$^{-/-}$ (n=6) mice was determined in metabolic chambers. P-value was determined by One-way Anova. (F) Rectal temperature of Sting$^{+/+}$ (n=13) and Sting$^{-/-}$ (n=14) mice. All graphs present means ± Standard Error of the Mean (SEM). P-value was determined by Student's t-test, unless otherwise stated. ns: not significant, *: P < 0.05, **P: < 0.01, ***P: < 0.001.

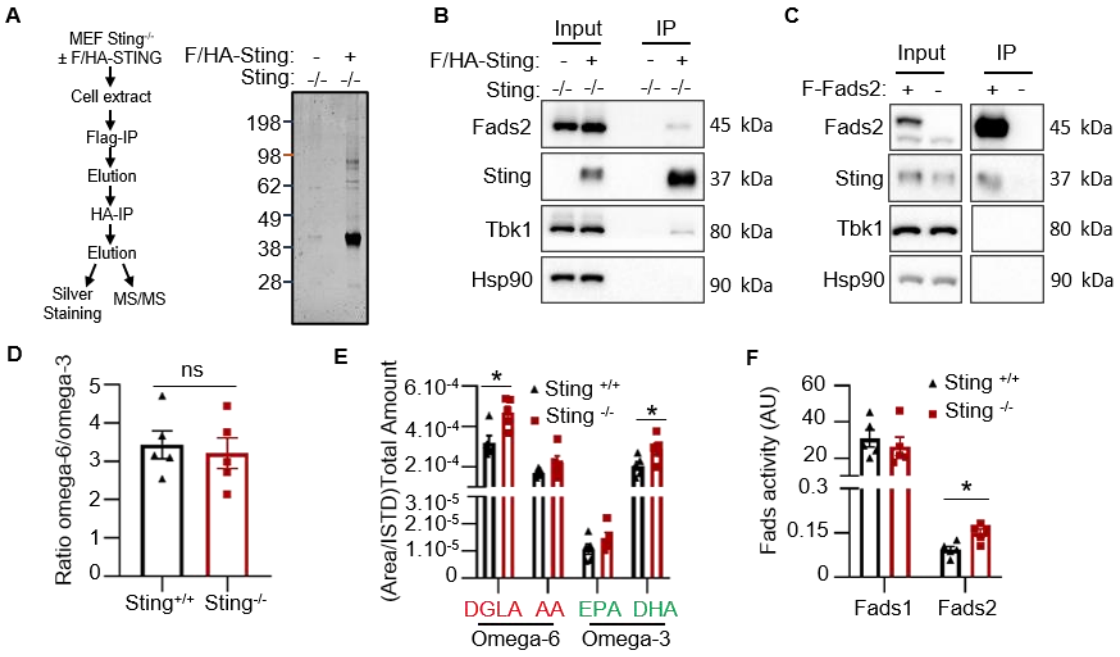

Fig. 2: Sting interacts with Fads2 and modulates polyunsaturated fatty acids pools.

(A) Left: Experimental scheme. Right: silver-staining of immunopurified Flag- and HA-tagged Sting (F/HA-Sting) separated on SDS-PAGE. Numbers on the left indicate the molecular weight in kDa. (B) Inputs and eluates from Flag-immunoprecipitated F/HA-Sting were analyzed by Western Blot (WB) using indicated antibodies. (C) Inputs and eluates from Flag-immunoprecipitated Flag-Fads2 were analyzed by WB using indicated antibodies. (D) Ratio between total Omega-6 and Omega-3 PUFAs and derivatives in liver samples (n=5). (E) PUFAs and derivatives were measured in Sting$^{+/+}$ (n=5) and Sting$^{-/-}$ (n=5) mice liver using LC-MS. Graph represents the sum of the indicated PUFA and their respective derivatives. In red are Omega-6 derivatives (LA) and in green are Omega-3 (ALA) derivatives. (F) Fads1 and 2 enzyme activity in livers of Sting$^{+/+}$ and Sting$^{-/-}$ mice was estimated by calculating the substrate/product ratio of PUFAs measured in (E). All graphs present means ± SEM. P-value was determined by Student's t-test. ns: not significant, *: $P < 0.05$.

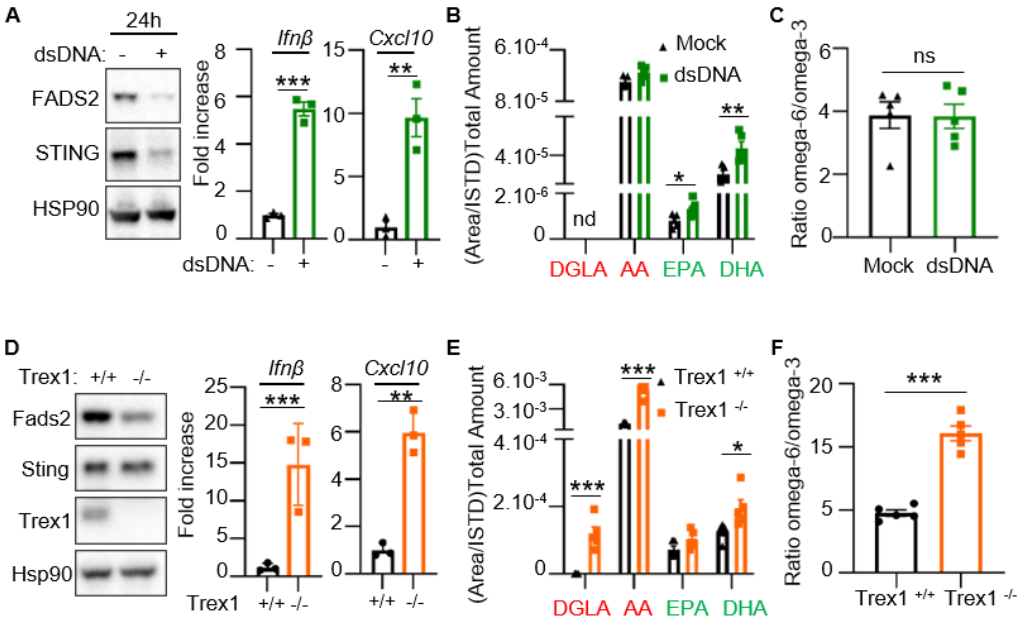

Fig. 3: Activation-dependent Sting degradation promotes Fads2 activity.

(A) Left: Whole cell extracts of 293T cells transfected or not with 2µg dsDNA for 6 or 24h were analyzed by WB using indicated antibodies. Right: *Ifnβ* and *Cxcl10* mRNA levels were measured by RT-qPCR (n=3). (B) Omega-6 and Omega-3 PUFAs and derivatives were measured in 293T cells transfected or not with 2µg dsDNA. Graph represents the sum of the indicated PUFA and their derivatives (n=5). (C) Ratio between total Omega-6 and Omega-3 PUFAs and derivatives in samples from (B). (D) Left: Whole-cell extracts from WT-MEF or MEF$^{Trex1-/-}$ were analyzed by WB using indicated antibodies. Right: *Ifnβ* and *Cxcl10* mRNA levels were measured by RT-qPCR in WT-MEF (n=3) and MEF$^{Trex1-/-}$ (n=3) MEFs. (E), n-6 and n-3 PUFAs and derivatives were measured in WT-MEF or MEF$^{Trex1-/-}$. Graph represents the sum of the indicated PUFA and their derivatives (n=5). (F) Ratio between total Omega-6 and Omega-3 PUFAs and derivatives in samples (n=5) treated as in (E). All graphs present means ± SEM. P-value was determined by Student's t-test. *: P < 0.05, **P: < 0.01, ***P: < 0.001.

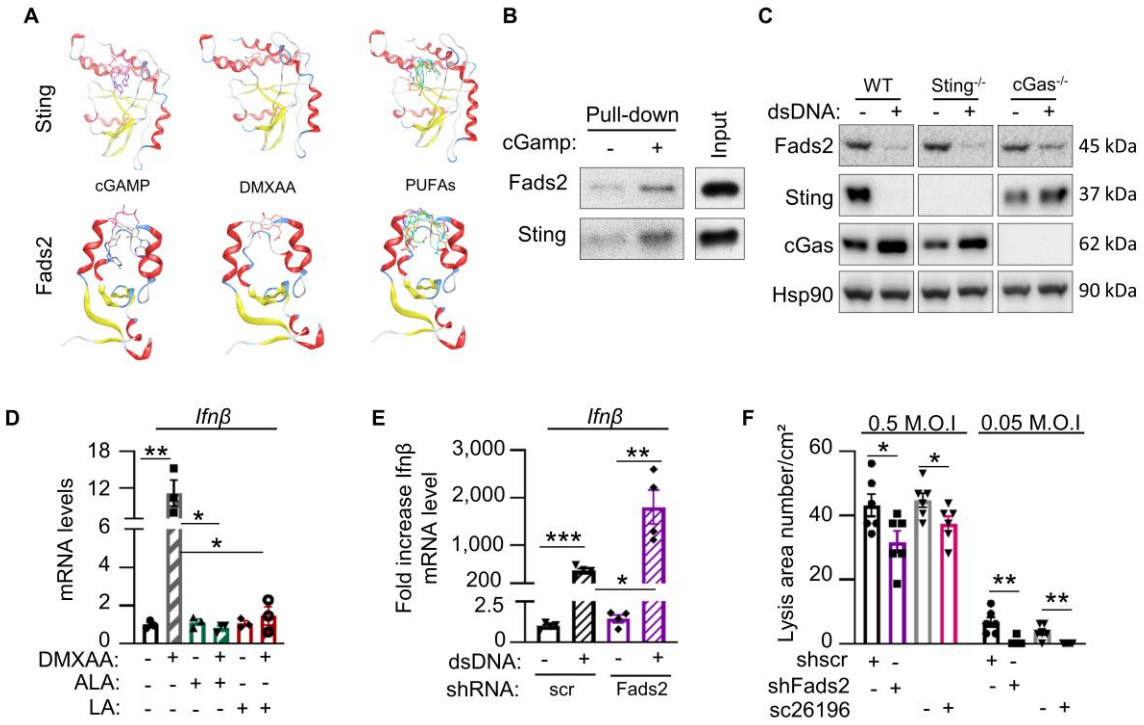

Fig. 4: cGAMP and PUFAs Orchestrate the Crosstalk between Fads2 and Sting.

(A) Molecular docking of cGAMP, DMXAA, and 6 PUFAs to STING (top) or FADS2 (bottom). Color coding for ligand is: LA in blue, ALA in green, AA in orange, DHA in turquoise, DGLA in brown and EPA acid in magenta. (B) Binding of Flag-purified F-Fads2 or F/HA-Sting to Streptavidin beads-immobilized biotinylated cGAMP was analysed by WB using anti-Sting or anti-Fads2 antibodies. (C) Whole cell extracts from WT, Sting$^{-/-}$, or cGas$^{-/-}$ MEF stimulated or not dsDNA (2µg) for 24 h were analyzed by WB using indicated antibodies. (D) WT-MEF were stimulated with DMXAA (100µM) in combination or not with ALA (50µM) or LA (50µM) for 2 h prior to RNA extraction and RT-qPCR analysis of *Ifnβ* mRNA levels. Graphs present fold increase *Ifnβ* as compared to unstimulated cells (n=3). (E) *Ifnβ* mRNA levels were measured by RT-qPCR in cells expressing Scramble (scr) or Fads2-targeting shRNAs after stimulation or not with dsDNA for 6 h (n=3). (F) WT-MEF were infected with HSV-KOS64 in presence of not of a Fads2 inhibitor (sc26196) for 90 min. Forty-eight h post infection, cells were fixed and stained with crystal violet and plaques counted. Plaques are presented as lysis area per cm^2. All graphs are means ± SEM from at least 3 independent experiments. P-value was determined by Student's t-test. *: P < 0.05, **: P < 0.01, ***: P < 0.001.